*Chinese Journal of*
**POLYMER SCIENCE**

ARTICLE

https://doi.org/10.1007/s10118-019-2300-6
*Chinese J. Polym. Sci.* **2020**, *38*, 100–108

# Nanoparticle Dispersion and Glass Transition Behavior of Polyimide-grafted Silica Nanocomposites

Sha-Ni Hu, Yu Lin*, and Guo-Zhang Wu*

*Shanghai Key Laboratory of Advanced Polymeric Materials, School of Materials Science and Engineering, East China University of Science and Technology, Shanghai 200237, China*

Electronic Supplementary Information

**Abstract** How to control the spatial distribution of nanoparticles to meet different performance requirements is a constant challenge in the field of polymer nanocomposites. Current studies have been focused on the flexible polymer chain systems. In this study, the rigid polyimide (PI) chain grafted silica particles with different grafting chain lengths and grafting densities were prepared by "grafting to" method, and the influence of polymerization degree of grafted chains ($N$), matrix chains ($P$), and grafting density ($\sigma$) on the spatial distribution of nanoparticles in the PI matrix was explored. The glass transition temperature ($T_g$) of PI composites was systematically investigated as well. The results show that silica particles are well dispersed in polyamic acid composite systems, while aggregation and small clusters appear in PI nanocomposites after thermal imidization. Besides, the particle size has no impact on the spatial distribution of nanoparticles. When $\sigma \cdot N^{0.5} \ll (N/P)^2$, the grafted and matrix chains interpenetrate, and the frictional resistance of the segment increases, resulting in restricted relaxation kinetics and $T_g$ increase of the PI composite system. In addition, smaller particle size and longer grafted chains are beneficial to improving $T_g$ of composites. These results are all propitious to complete the microstructure control theory of nanocomposites and make a theoretical foundation for the high performance and multi-function of PI nanocomposites.

**Keywords** Polyimide grafted nanoparticle; Dispersion morphology; Glass transition temperature

**Citation:** Hu, S. N.; Lin, Y.; Wu, G. Z. Nanoparticle dispersion and glass transition behavior of polyimide-grafted silica nanocomposites. *Chinese J. Polym. Sci.* **2020**, *38*, 100–108.

## INTRODUCTION

Polymer nanocomposites (PNCs) combine the excellent properties of inorganic nanoparticles (NPs) and polymers to exhibit superior performance. Considerable efforts have been focused on regulating the specific dispersion of NPs in PNCs to achieve the desired performance,[1–4] but finding the intrinsic association of interfacial interactions with the spatial distribution of NPs and macroscopic properties of materials has always been an enormous challenge.[5,6] The unsolved issues hinder the understanding of substantial relationship between the dispersion of NPs and the properties of PNCs, thus limiting the wide application of such materials.

Previous studies have demonstrated that the interfacial interaction between NPs and polymers is the key to regulating the dispersion of NPs. One of the most effective approaches to achieve the specific NPs dispersion state is grafting polymer chains on the surface of NPs. According to the existing studies,[7–13] the self-assembled anisotropic structures of NPs are determined by the ratio of the degree of polymerization of the matrix ($P$) to the grafted chain ($N$), as well as the grafting density ($\sigma$). However, the experiments and theoretical simulations have been focused on polystyrene (PS), poly(ethylene oxide) (PEO), and other flexible chain systems,[2,8,14–18] but not yet involved the rigid ones. Importantly, since the rigid chains show difficulties in chain packing compared with the flexible ones, the penetration between the rigid grafted and matrix chains must be distinct from that between the flexible ones, which possibly causes abnormal changes in condensed structures of rigid chain grafted-NPs and is worthy of further exploration.

As a basic physical property of materials, the glass transition temperature ($T_g$) plays an indispensable role in macroscopic properties of PNCs. Generally, the interfacial interactions between NPs and polymer matrix greatly affect $T_g$.[19–23] The NP-polymer interfacial interactions can either promote or inhibit the segmental mobility of PNCs,[24,25] resulting in a decrease[22] or an increase[24,26,27] of $T_g$. However, the grafted NP filled PNCs show more challenge in exploration of glass transition behavior due to complex interactions between grafted and matrix chains.[1,6,28] It has been reported that $T_g$ of the grafted NP-filled PNCs was influenced by the values of $P$, $N$, and $\sigma$, as well as the particle size.[1,29] It must be pointed out

* Corresponding authors, E-mail: linyu@ecust.edu.cn (Y.L.)
E-mail: wgz@ecust.edu.cn (G.Z.W.)

Received April 7, 2019; Accepted May 20, 2019; Published online August 30, 2019

that the difference of chain packing between the PNCs filled by rigid chain grafted NP and the flexible ones may influence the glass transition behavior, which remains to be studied.

As one of the most excellent engineering polymers, polyimide (PI) has attracted great interest in high-tech fields such as aerospace and microelectronics due to its high temperature and radiation resistance, along with high strength and modulus.[30–36] PI nanocomposites can further broaden the optical, electrical, and magnetic properties of the neat matrix.[37] For example, the development of highly dielectric or high-insulation materials requires uniform dispersion of NPs,[38] while the NPs are required to form a regular three-dimensional network structure in PI nanocomposites for transparent conductive films and high-strength heat-conducting materials.[39,40] Therefore, achieving controllable distribution of NPs in the PI matrix is a valuable but challengeable approach for realizing the desired multi-functionalization of PI nanocomposites. However, due to the rigid structure of PI chains, related research on the spatial distribution regulation of NPs in the PI matrix has not been reported.

In this study, the "grafting to" method was used to synthesize PI-grafted silica NPs, which was filled into PI matrix to construct a model system to study the effect of $N$ and $\sigma$ on the spatial distribution of NPs in the rigid chain system. $T_g$ of the composite system was further investigated, which revealed the contribution of interactions between the rigid grafted and matrix chains, as well as the particle size, to the glass transition behavior.

## EXPERIMENTAL

### Materials

Hydrophilic fumed silica NPs with an average primary particle diameter of 15 nm were purchased from Hangzhou Wanjing New Material Co., Ltd. China. The coupling agent γ-triethoxysilylpropylamine (APTES) was purchased from Nanjing Daoning Chemical Co., Ltd. China. The respective dianhydride and diamine monomers of 4,4′-(hexafluoroisopropylidene)diphthalic anhydride (6FDA) and 4,4′-diaminodiphenyl ether (ODA) were purchased from Changzhou Yang Guang Pharmaceutical Co., Ltd. The molecular structures of the investigated PI are shown in Scheme 1. Anhydrous *N*-methylpyrrolidone (NMP), *N*,*N*-dimethylacetamide (DMAc), and *N*,*N*-dimethylformamide (DMF) were obtained from Shanghai Titan Chemical Co., Ltd.

### Synthesis of Amino-functionalized Silica NPs

Silica particles (4 g) were treated using γ-triethoxysilylpropylamine (APTES) (0.2 g) in 100 mL of toluene under stirring and ultrasonic dispersion. The mixture was transferred into a 250 mL three-neck round-bottom flask and the reaction was performed at 50 °C for 24 h in a water bath. After reaction, the suspension containing APTES modified $SiO_2$ ($SiO_2$-APTES) was centrifuged at 14500 r·min$^{-1}$ for 10 min and the precipitates were washed three times with ethanol in order to remove the excess APTES. The deposit was dried to constant weight in a vacuum oven at 80 °C for 24 h.

### Synthesis of PI-grafted Silica NPs

First of all, PI with various molecular weights was synthesized according to the simple reaction reported by Ragosta,[41] as shown in Scheme 1. The molecular weight of PI was controlled by adjusting the molar ratio of 6FDA (*m*) to ODA (*n*) monomers (*m*/*n*) (1/1, 1/0.95, 1/0.90).[42] As an example, 6FDA (0.01 mol) was slowly added with stirring after ODA (0.01 mol) was completely dissolved in the NMP solvent. After reacting for 5 h in an ice water bath, a poly(amic acid) (PAA) solution with a solid content of 10 wt% was formed. The solution was diluted with NMP and poured into a petri dish. Then, the PAA film was prepared after slow evaporation of solvent at 80 °C to 150 °C for 24 h. Afterwards, the film was thermally imidized stepwise at 200, 250, and 300 °C for 1 h at each temperature.

Grafted polymer chains were grown from the particle surface using "grafting to" methord as shown in Scheme 2. The procedure is as follows. PI (3 g) was dissolved in 200 mL of DMAc and stirred at 80 °C for 2 h, while amino-functionalized silica NPs (1 g) were dispersed in 100 mL of DMAc. Once dissolution was complete, the solution was mixed with dispersions and transferred into a 500 mL three-neck round-bottom flask and the reaction was performed at 60 °C for 24 h in a water bath. Afterwards, the slurry mixture was centrifuged and washed several times with DMAc and ethanol, and then

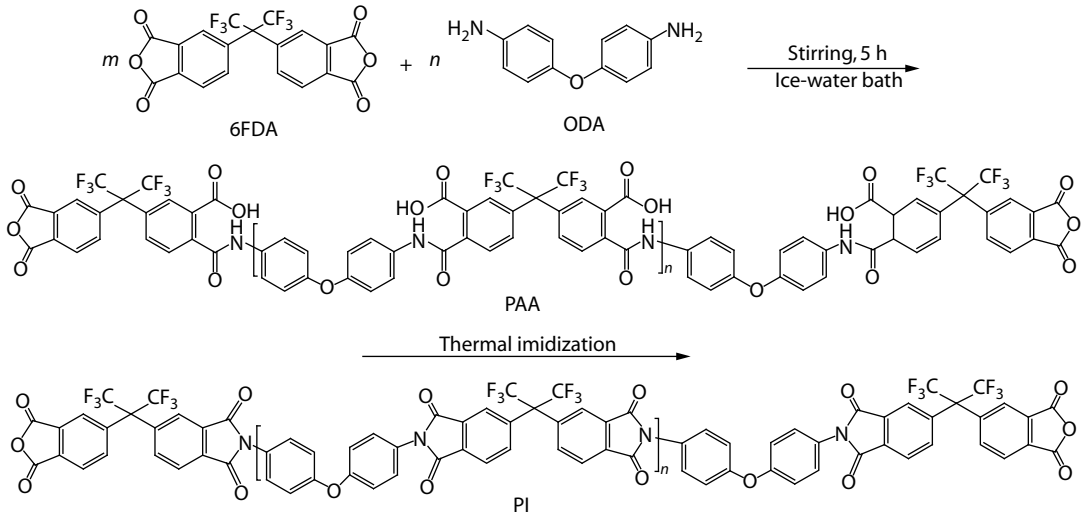


**Scheme 1** Schematic representation of synthesis procedure for PI.

https://doi.org/10.1007/s10118-019-2300-6

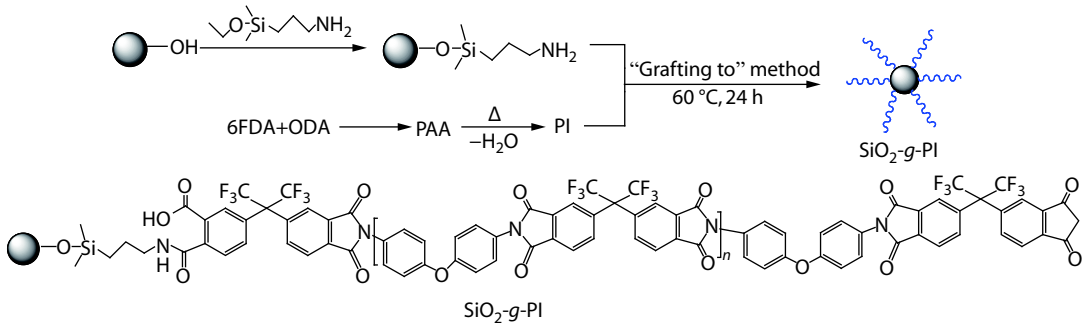


**Scheme 2** Schematic representation of synthesis procedure for PI-grafted silica NPs.

dried in a vacuum oven at 100 °C for 24 h. The finally obtained grafted silica NPs were named in the form of $SiO_2$-*g*-$PI_x$, where *x* represents the number-average molecular weight of the grafted PI chains.

### Preparation of Silica NP-filled PNCs

According to the previous preparation of PI films, we found that only a ratio of *m*/*n* = 1/1 ensured good integrity of the PI film, while the other two PI films (*m*/*n* = 1/0.95, 1/0.90) were relatively brittle due to their lower molecular weights, thus affecting the subsequent tests. To ensure the machinability of PI film, the PI matrix with the high molecular weight (*m*/*n* = 1/1) was adopted. Grafted or ungrafted silica NPs with the desired weight and PAA (*m*/*n* = 1/1) were mixed into NMP with a total solid weight fraction of 5 wt%, 7.5 wt%, and 10 wt%. After thorough stirring and dispersion, the composite PAA and PI films were fabricated with the same procedure of preparing neat PAA and PI films described above. The final thickness of the films was about 0.2 mm.

### Characterization of $SiO_2$-*g*-PI Composite NPs and PNCs

FTIR measurements were performed by using a Nicolet 5700 FTIR spectrometer to investigate the grafting structure of $SiO_2$-*g*-PI composite NPs. A small amount of sample powder was mixed with potassium bromide, ground, and compressed into tablets. The wavenumber was scanned from 4000 $cm^{-1}$ to 400 $cm^{-1}$ for 32 times. The spectra were obtained in transmittance mode in the wavenumber range of 400–4000 $cm^{-1}$. X-ray photoelectron spectroscopy (XPS) measurement was performed using a ESCALAB 250Xi spectrometer. The final amount of APTES and grafted PI chains on silica surfaces was determined by thermogravimetric analysis (TGA, Netzsch STA 409) from 50 °C to 800 °C at a heating rate of 10 °C·$min^{-1}$ in a nitrogen atmosphere. The molecular weight and polydispersity index (PDI) of grafted and matrix PI chains were characterized in DMF solution by using a gel permeation chromatograph (GPC, Waters 1515) equipped with a 79911GP-MXC column. A polymer solution with a concentration of 0.5 mg·$mL^{-1}$ was prepared using a solvent DMF at a flow rate of 1.0 mL·$min^{-1}$. A transmission electron microscope (TEM, JEM 1400) was used to observe the silica NP distribution in PNCs. The composite film was cut into one piece, embedded in epoxy resin, and subjected to ultrathin sectioning. The dispersion state of the NPs was observed by TEM. Differential scanning calorimetry (DSC, TA DSC25) was utilized to examine $T_g$ of the grafted and ungrafted NP filled PNCs. The samples were heated from 40 °C to 350 °C at 10 °C·$min^{-1}$, kept for 5 min to eliminate the heat history, then cooled down to 200 °C and reheated up to 350 °C at 10 °C·$min^{-1}$. The second heating scan data were adopted.

## RESULTS AND DISCUSSION

### Characterization of Grafted Silica NPs

Fig. 1 shows FTIR spectra of bare, APTES-modified, and PI-grafted silica NPs. As shown in Fig. 1(a), compared to the bare silica, $SiO_2$-APTES exhibits new absorption bands at 2852, 2927, and 2962 $cm^{-1}$, which correspond to C—H, —$CH_2$—, and —$CH_3$ stretching of APTES, respectively,[43] indicating the successful modification of silica NPs. The characteristic absorption bands

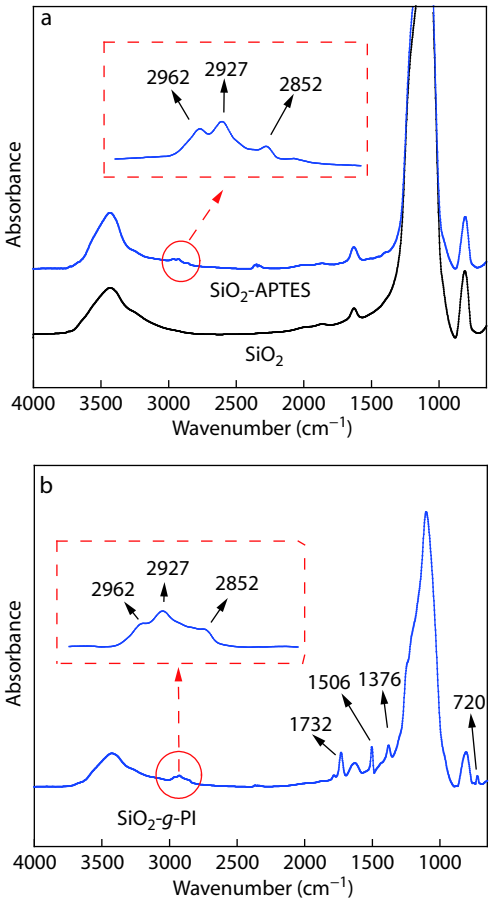


**Fig. 1** FTIR spectra of (a) bare $SiO_2$, $SiO_2$-APTES, and (b) $SiO_2$-*g*-PI composite particles.

of PI can be observed from the spectra of $SiO_2$-*g*-PI as shown in Fig. 1(b), including the bending vibration of N—H group at 720 $cm^{-1}$, stretching vibration of imide group (—CONOC—) at 1376 $cm^{-1}$, and *p*-substituted benzene vibration peak at 1506 $cm^{-1}$ as well as the absorption band of C=O group at 1732 $cm^{-1}$. The ungrafted and physically adsorbed PI chains were removed by DMAc solvent rinsing, so the FTIR spectra verify that the PI chains are successfully grafted onto the surface of $SiO_2$-APTES NPs.

To further elucidate the chemical bonding rather than physical absorption of the PI chains on the surface of silica NPs, $SiO_2$-*g*-PI samples were analyzed by XPS based on chemical shift observations. Fig. 2(a) shows the XPS C1s and N1s spectra of $SiO_2$-*g*-PI NPs. From Fig. 2(a), the $SiO_2$-*g*-PI C1s XPS spectrum shows representative peaks of C—N, C—O—C, C=O, and —$CF_3$ at 285.6, 286.4, 288.8, and 293.4 eV, respectively, corresponding to the characteristic peaks of PI.[44,45]

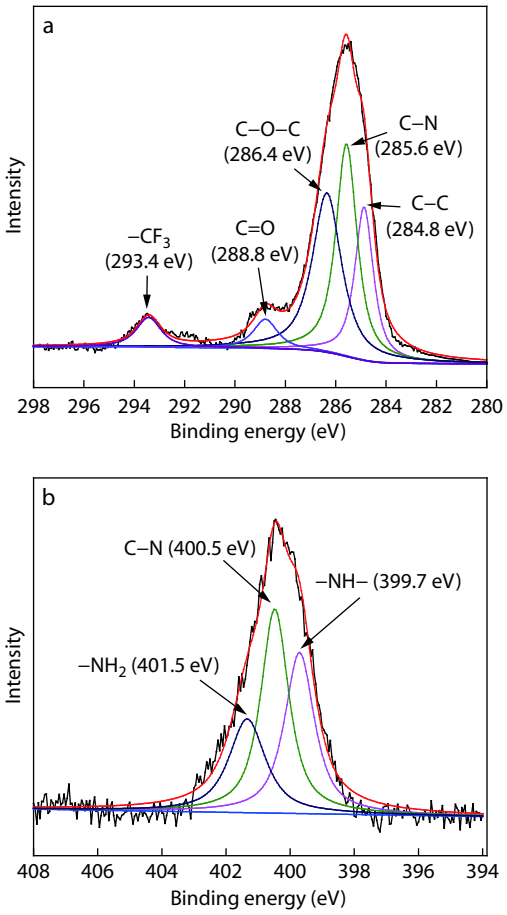


**Fig. 2** High resolution (a) C1s XPS spectrum and (b) N1s XPS spectrum of $SiO_2$-*g*-PI NPs.

Moreover, the N1s XPS spectrum of $SiO_2$-*g*-PI shown in Fig. 2(b) presents peaks at 399.7, 400.5, and 401.5 eV, which are assigned to N—H, C—N, and —$NH_2$, respectively, implying a reaction between the amine functional group and anhydride group of PI molecules (see Scheme 2). The above-mentioned XPS results further demonstrate that $SiO_2$ was chemically functionalized by PI chains, which agrees well with the FTIR results.

Fig. 3 shows the TGA curves of bare, APTES modified, and PI grafted silica NPs, which are used for quantitative calculation of grafting ratio and $\sigma$. It can be found that bare $SiO_2$ has a weight loss of around 2% below 100 °C attributed to the hydroxyl groups of water adsorbed onto the silica surface, and further weight decrease is related to the dehydroxylation of Si—OH group. According to the TGA experimental data, the increased weight loss is due to the decomposition of coupling agent molecules for modified $SiO_2$-ATPES while it is ascribed to the degradation of grafted PI chains at 480–630 °C for $SiO_2$-*g*-PI NPs, indicating the successful attachment *via* "grafting to" method. The grafting ratio can be obtained by TGA residues, and $\sigma$, defined as the number of polymer chains per unit surface area of NPs, can be calculated as follows:[11]

$$\sigma = g_d D \rho_p N_A / 6 M_g \quad (1)$$

where $g_d$ is the grafting degree, $D$ is the diameter of NPs, $\rho_P$ is the NP density, $N_A$ is Avogadro's number, and $M_g$ is the grafted chain molecular weight. Table 1 lists $\sigma$ of various $SiO_2$-*g*-PI NPs in detail, being 0.0120, 0.0055, and 0.0016 chains·$nm^{-2}$ for $SiO_2$-*g*-$PI_{18k}$, $SiO_2$-*g*-$PI_{37k}$, and $SiO_2$-*g*-$PI_{61k}$, respectively. These values are consistent with the reported "grafting to" method with low $\sigma$[46–48] and lower than that of flexible chain grafted NPs in our previous study.[3,6] In addition, $\sigma$ decreases with the increase of grafted chain length, which is limited by the steric effect of "grafting to" method.[49–51] That is, the entanglement

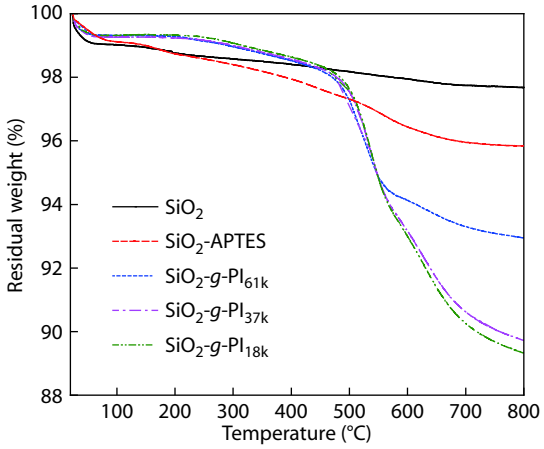


**Fig. 3** TGA curves for bare $SiO_2$ and functionalized $SiO_2$ with APTES and $SiO_2$-*g*-PI particles.

**Table 1** The molar ratio of 6FDA (*m*) to ODA (*n*) monomers (*m*/*n*), molecular weight ($M_n$) of grafted PI chains, degree of polymerization of the matrix (*P*) and the grafted (*N*) chains, and grafting density ($\sigma$).

| Sample | NP code | *m*/*n* | $M_n$ (g·$mol^{-1}$) | PDI | *P* | *N* | $\sigma$ ($nm^{-2}$) | $\sigma \cdot N^{0.5}$ | $1/\alpha$ (*P*/*N*) | $(N/P)^2$ |
|---|---|---|---|---|---|---|---|---|---|---|
| 1 | $SiO_2$-*g*-$PI_{61k}$ | 1/1 | 61k | 3.16 | 95 | 95 | 0.0016 | 0.02 | 1 | 1 |
| 2 | $SiO_2$-*g*-$PI_{37k}$ | 1/0.95 | 37k | 1.75 | 95 | 57 | 0.0055 | 0.04 | 1.65 | 0.37 |
| 3 | $SiO_2$-*g*-$PI_{18k}$ | 1/0.90 | 18k | 2.07 | 95 | 28 | 0.0120 | 0.06 | 3.39 | 0.29 |

https://doi.org/10.1007/s10118-019-2300-6

of already grafted chains hinders the free chains from branching onto the surface of NPs, resulting in the low $\sigma$. Moreover, the rigid structure of grafted PI chains is also one of the reasons for low $\sigma$.

## Dispersion Morphology of PI Grafted Silica NPs in PI Matrix

Due to the high temperature thermal imidization of PI during the synthesis process, which involves the structural change and thermal annealing, the dispersion of NPs in the PAA matrix may be different from that in the PI matrix. Fig. 4 shows the dispersion morphology of bare $SiO_2$ and the grafted silica NPs with 10 wt% content in the PAA matrix. It is obvious that the ungrafted (Fig. 4a) and the grafted (Fig. 4b) NPs both exhibit a well dispersed state in the matrix. These results indicate that the NPs do not tend to form aggregates prior to thermal imidization and the reason will be discussed below.

Fig. 5 shows the TEM images of PI/$SiO_2$ and PI/$SiO_2$-*g*-PI composites with a silica content of 10 wt% which demonstrate the totally distinct dispersion morphology compared

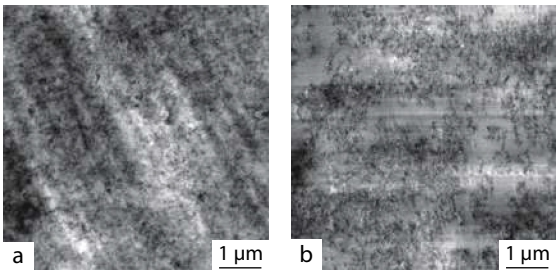


**Fig. 4** TEM images of (a) $SiO_2$ and (b) $SiO_2$-*g*-$PI_{61k}$ NPs filled in PAA composites. The content of silica NPs is 10 wt%. Note that a well dispersed state can be seen in both the bare and grafted silica NP filled PAA composites.

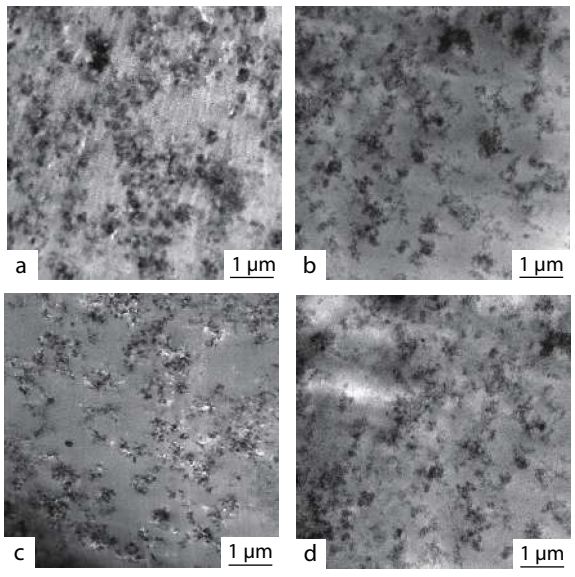


**Fig. 5** TEM images of (a) $SiO_2$, (b) $SiO_2$-*g*-$PI_{18k}$, (c) $SiO_2$-*g*-$PI_{37k}$, and (d) $SiO_2$-*g*-$PI_{61k}$ NPs filled PI composites with a silica content of 10 wt%. Large NP agglomerates can be seen in the bare silica filled PI system, while small clusters can be observed in the grafted silica NP filled PI composites.

with the PAA composites. It is found that the NPs exhibit a larger cluster in the bare silica NP-filled system, as shown in Fig. 5(a), because of the large specific surface area and interface energy of bare silica as well as the strong enthalpy attraction. The grafted NPs are all uniformly dispersed in the form of small clusters in $SiO_2$-*g*-$PI_{18k}$, $SiO_2$-*g*-$PI_{37k}$, and $SiO_2$-*g*-$PI_{61k}$ NP filled composites, as shown in Figs. 5(b)–5(d), which are not affected by the grafted chain length. To compare with the spatial distribution of classical phase diagrams from literature,[8] they are expected to appear as not only the small clusters but also the connected sheet structures, as shown in Fig. 6. The "grafting to" method is limited to the preparation of grafted NPs with a low $\sigma$, which causes the difficulty to achieve a good dispersion spatial distribution of the grafted NPs in the matrix.[2] Besides, the assembled anisotropic structures of grafted NPs in the matrix are essentially attributed to the diffusion and penetration between chains; the rigid structure of grafted and matrix chains may suppress diffusion, thus limiting the possibility of spatial dispersion such as string and connected sheets. In order to investigate the effect of NP content on the dispersion morphology, TEM images of bare and grafted NPs filled PI composites with a silica content of 5 wt% are shown in Fig. S1 (in the electronic supplementary information, ESI). The results also show that the large NP agglomerates and small clusters can be observed in bare and grafted NP filled PI composites, respectively, indicating that the silica content has no effect on the dispersion morphology of NPs.

The size distributions of particle agglomerates and their average diameters could be estimated through image analysis and data statistics based on the TEM micrographs. The obtained distributions of SiO2-*g*-$PI_{61k}$ in PAA and PI matrix are presented in Fig. S2 (in ESI). It can be noted that the size dis-

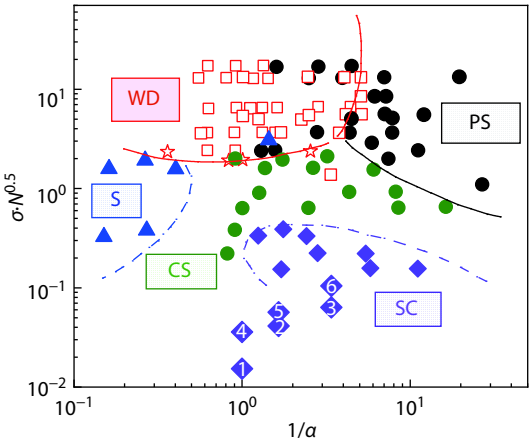


**Fig. 6** The dispersion morphologies of PI nanocomposites in the classical composite morphology diagram created from reference. (Reproduced with permission from Ref. [8]; Copyright (2013) American Chemical Sciely). The points, adapted from the literature, are symbol coded so that the open square symbols (□) correspond to well dispersed particles (WD), black solid circle symbols (●) to phase separated samples (PS), solid triangle symbols (▲) to strings (S), green solid circle symbols (●) to connected sheets (CS), and solid diamond symbols (◆) to small clusters (SC). The numbered points of 1–3 are experimental data in this study, corresponding to their sample numbers, while the number of 4–6 corresponds to the sample of 1–3 in our previous study,[52] respectively.

https://doi.org/10.1007/s10118-019-2300-6

tribution of grafted NPs in PAA matrix (Fig. S2a, in ESI) is narrower than that of NPs in PI matrix (Fig. S2b, in ESI), indicating a more uniform size of grafted NP agglomerates in PAA matrix. Besides, compared to the size of NP agglomerates in PI composite, the average diameter of NP agglomerates in PAA matrix is significantly smaller, further confirming that the NPs tend to aggregate into clusters after thermal imidization.

The great distinction in the dispersion morphology of NPs between PAA and PI composites is attributed to the difference in solvent effect and the thermal imidization process. Compared to PI composites, faster diffusion and motion of NPs in PAA composites are expected owing to the lower viscosity of PAA. Hence, the relatively uniform dispersion of silica NPs in PAA matrix can be attributed to the stabilizing effect of solvent. Besides, low drying temperature during solvent evaporation also contributes to the well dispersed morphology. Conversely, the high-temperature thermal imidization is related to the process of thermal annealing, which leads to the aggregation and anisotropic self-assembled structure[2,8] of NPs in PI composites. Therefore, the NPs self-assemble into small clusters and large aggregate structures in PI composites because of the high temperature.

In order to study the influence of NP size on the dispersion morphology of NPs, PI composites of larger particle with diameter of 30 nm in our previous study[52] are compared to as-prepared composites in this study. With similar values of $P/N$ and $\sigma$, the grafted and ungrafted NPs of different diameters exhibit the same dispersed morphology in the composite melt, that is, the large clusters for bare silica NP-filled PNCs and small clusters for grafted silica-filled composites. In our previous study,[3] the thermodynamically stable state of PS-grafted silica NP distribution is merely related to $N$ and $\sigma$, and independent of the particle size within the range of 15–65 nm. Magdalena and co-workers[53] also found that isotactic polypropylene grafted silica NPs exhibit the unchanging dispersion morphology when the particle size is between 12–40 nm. In this study, the spatial distribution of PI-grafted NPs is also unaffected by the particle size within a certain range (15–30 nm), which is consistent with the result of flexible chain systems. However, much more work should be done to verify whether it is applicable to larger or smaller NPs. Moreover, the spatial distribution of PI grafted-silica NPs in the classic phase diagram is summarized in Fig. 6. In the figure, the abscissa represents the ratio of molecular chain length ($P/N = 1/\alpha$), while the ordinate reflects the extent of crowding of the grafted chain ($\sigma \cdot N^{0.5}$). Similarly, connected sheets and small clusters morphologies are both expected to appear for grafted silica NPs. The absence of connected sheets morphologies is attributed to the rigidity of grafted and matrix PI chains. The results further illustrate that the spatial distribution of rigid chain grafted NPs is different from that of flexible chain systems.

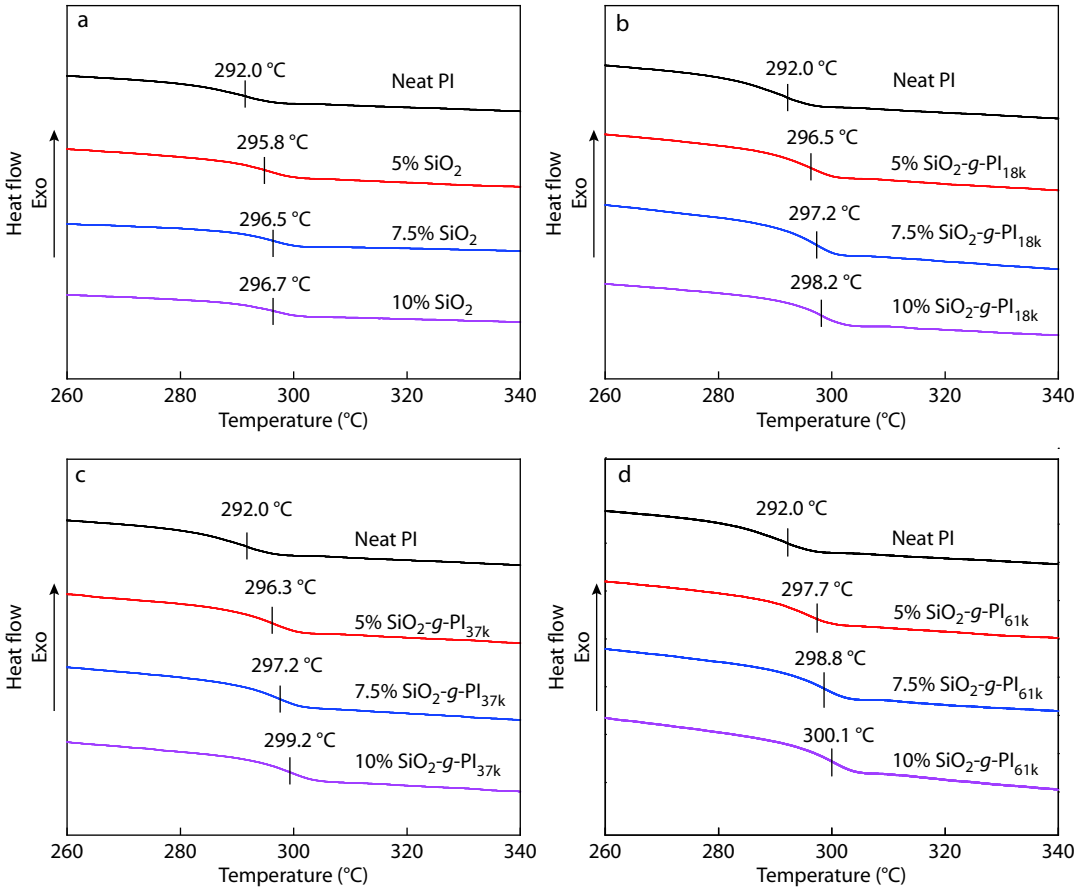


**Fig. 7** DSC curves of (a) $SiO_2$, (b) $SiO_2$-$g$-$PI_{18k}$, (c) $SiO_2$-$g$-$PI_{37k}$, and (d) $SiO_2$-$g$-$PI_{61k}$ particles filled PI composites with various silica NP contents.

https://doi.org/10.1007/s10118-019-2300-6

### Glass Transition Behavior of Nanocomposites

The interfacial interactions between NP and the polymer matrix not only affect the spatial distribution of NPs, but also influence the glass transition behavior of PNCs. Fig. 7 shows the DSC curves of PI nanocomposites with various loading of grafted and ungrafted silica NPs. Compared with neat PI, both grafted and ungrafted NPs filled PNCs show a trend of increased $T_g$. Besides, $T_g$ increases with increasing the content of silica NPs.

The higher $T_g$ for PI/$SiO_2$ nanocomposites (Fig. 7a) is endowed by the hydrogen bonding interactions of tightly "bound layer" between polymer chains and hydrophilic silica NP surfaces,[27] while the increased $T_g$ for PI/$SiO_2$-*g*-PI nanocomposites (Figs. 7b–7d) is attributed to the interfacial interactions between the grafted and matrix PI chain. According to the previous reports,[1,54,55] there exist mutual diffusion and interpenetration between the grafted and matrix chains while $\sigma \cdot N^{0.5} \ll (N/P)^2$, and the frictional resistance during the movement of interface layer will be enhanced, which leads to an increased $T_g$. The $\sigma \cdot N^{0.5}$ and $(N/P)^2$ values of PI/$SiO_2$-*g*-PI composites in this study are calculated, as shown in Table 1. It is found that they all satisfy the condition of $\sigma \cdot N^{0.5} \ll (N/P)^2$, so the mutual penetration between PI grafted and matrix chains leads to the increase of $T_g$ in the resultant composites.

To further intuitively compare the changes in $T_g$, the $T_g$ deviations of the PI nanocomposites are summarized in Fig. 8, where $\Delta T_g(\varphi) = T_g(\varphi) - T_g^{PI}$ is plotted on the ordinate and the content of $SiO_2$ NPs ($\varphi$) is plotted on the abscissa. It is noteworthy that $\Delta T_g$ increases with increasing $\varphi$. Bare silica filled PNCs show obvious increase of $\Delta T_g$ in the case of low $\varphi$, but slight shifts of $\Delta T_g$ for high $\varphi$, which results from the aggregation of NPs in high loading as shown in Fig. 5(a). And $\Delta T_g$ of PI/$SiO_2$-*g*-PI systems remains higher than PI/$SiO_2$ composites because of the stronger interactions between grafted and matrix PI chains. Besides, with the increase of the molecular weight of grafted chains, $\Delta T_g$ increases more significantly for fixed $\varphi$. It was reported[9] that the growth of grafted chains (increase of *N*) leads to an enhancement in the interpenetration between the grafted and the matrix chains, creating a stronger interface. Moreover, the enhanced interpenetration between the long grafted and matrix chains will cause the reduced conformational entropy of grafted chains due to further stretching, so the grafted chains occupy a greater volume fraction of the nanocomposites. Both effects can lead to the reduced mobility of the polymer chains and higher $T_g$ of PI nanocomposites.

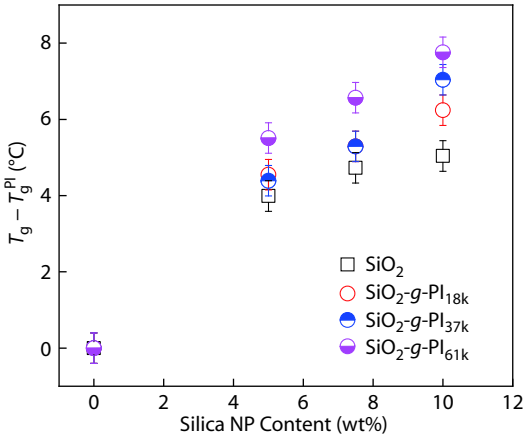


**Fig. 8** Changes in $T_g$ of PI nanocomposites as a function of silica NP weight fraction.

NPs with different sizes have various specific surfaces, which affects the enthalpy attraction between them, thus influences the interaction energy between NPs and the matrix polymer, and eventually leads to the changes in $T_g$ of the composites. The $T_g$ deviations of larger particles filled PI nanocomposites have been summarized in our previous study,[52] which are compared to the smaller one filled systems in this study to investigate the effect of particle size on the glass transition behavior. Obviously, the smaller particle size packed PI nanocomposites (Fig. 8) in this study perform better regulation of $\Delta T_g$ than the larger ones in the previous study. As the particle size of the NPs decreases, the specific surface area increases, which leads to reduced crowding of grafted chains on the surface and the enhanced interactions between the matrix chain and NPs, thus resulting in the limited movement of the surrounding segments of NPs and higher $T_g$ of nanocomposites.[56]

## CONCLUSIONS

$SiO_2$-*g*-PI NPs with low grafting density were prepared by "grafting to" method, and the *N*, *P*, and $\sigma$ values were controlled by regulating the monomer ratio. The NPs are well dispersed in the PAA matrix. However, due to the rigidity of PI grafted and matrix chains, as well as the influence of thermal annealing process, the grafted NPs only exhibit small clusters structure in the PI composites. In addition, the NP size has no effect on the dispersion morphology of silica NPs in the PI composites. Importantly, $T_g$s of the resulting composites are significantly improved, especially for the PI grafted silica-filled composites owing to the interfical interactions. Moreover, $T_g$ increases more obviously as the grafted chain length increases and the NP size decreases.

### Electronic Supplementary Information

Electronic supplementary information (ESI) is available free of charge in the online version of this article at http://dx.doi.org/10.1007/s10118-019-2300-6.


## ACKNOWLEDGMENTS

This work was financially supported by the National Natural Science Foundation of China (Nos. 51503066 and 51873063), the National Basic Research Program of China (No. 2013CB035505), Shanghai Sailing Program (No. 14YF1404900), and MOE Key Laboratory of Macromolecular Synthesis and Functionalization, Zhejiang University (No. 2017MSF02).


## REFERENCES


1 Oh, H.; Green, P. F. Polymer chain dynamics and glass transition in athermal polymer/nanoparticle mixtures. *Nat. Mater.* **2009**, *8*, 139–143.

2 Akcora, P.; Liu, H.; Kumar, S. K.; Moll, J.; Li, Y.; Benicewicz, B. C.;

Schadler, L. S.; Acehan, D.; Panagiotopoulos, A. Z.; Pryamitsyn, V. Anisotropic self-assembly of spherical polymer-grafted nanoparticles. *Nat. Mater.* **2009**, *8*, 354–359.
3 Liu, L. P.; Lin, Y.; Guan, A. G.; Wu, G. Z. Tuning spatial distribution of polystyrene-grafted silica nanoparticles in different polymer matrices. *Acta Polymerica Sinica* (in Chinese) **2016**, 1546–1554.
4 Tan, Y. Q.; Wang, L. B.; Xiao, J. L.; Zhang, X.; Wang, Y.; Liu, C.; Zhang, H. W.; Liu, C. Z.; Xia, Y. Z.; Sui, K. Y. Synchronous enhancement and stabilization of graphene oxide liquid crystals: inductive effect of sodium alginates in different concentration zones. *Polymer* **2019**, *160*, 107–114.
5 Mackay, M. E.; Tuteja, A.; Duxbury, P. M.; Hawker, C. J.; Van, H. B.; Guan, Z.; Chen, G.; Krishnan, R. S. General strategies for nanoparticle dispersion. *Science* **2006**, *311*, 1740–1743.
6 Lin, Y.; Liu, L. P.; Zhang, D. G.; Liu, Y. H.; Guan, A. G.; Wu, G. Z. Unexpected segmental dynamics in polystyrene-grafted silica nanocomposites. *Soft Matter* **2016**, *12*, 8542–8553.
7 Green, P. F. The structure of chain end-grafted nanoparticle/homopolymer nanocomposites. *Soft Matter* **2011**, *7*, 7914–7926.
8 Kumar, S. K.; Jouault, N.; Benicewicz, B.; Neely, T. Nanocomposites with polymer grafted nanoparticles. *Macromolecules* **2013**, *46*, 3199–3214.
9 Sunday, D. F.; Green, D. L. Thermal and rheological behavior of polymer grafted nanoparticles. *Macromolecules* **2015**, *48*, 8651–8659.
10 Xue, Y. H.; Zhu, Y. L.; Quan, W.; Qu, F. H.; Han, C.; Fan, J. T.; Liu, H. Polymer-grafted nanoparticles prepared by surface-initiated polymerization: the characterization of polymer chain conformation, grafting density and polydispersity correlated to the grafting surface curvature. *Phys. Chem. Chem. Phys.* **2013**, *15*, 15356–15364.
11 Hasegawa, R.; Aoki, Y.; Doi, M. Optimum graft density for dispersing particles in polymer melts. *Macromolecules* **1996**, *29*, 6656–6662.
12 Ndoro, T. V. M.; Voyiatzis, E.; Ghanbari, A.; Theodorou, D. N.; Böhm, M. C.; Müller-Plathe, F. Interface of grafted and ungrafted silica nanoparticles with a polystyrene matrix: atomistic molecular dynamics simulations. *Macromolecules* **2011**, *44*, 2316–2327.
13 Mansoori, Y.; Roojaei, K.; Zamanloo, M. R.; Imanzadeh, G. Polymer-clay nanocomposites: chemical grafting of polystyrene onto Cloisite 20A. *Chinese J. Polym. Sci.* **2012**, *30*, 815–823.
14 Chevigny, C.; Dalmas, F.; Cola, E. D.; Gigmes, D.; Bertin, D.; Boué, F.; Jestin, J. Polymer-grafted-nanoparticles nanocomposites: dispersion, grafted chain conformation, and rheological behavior. *Macromolecules* **2011**, *44*, 122–133.
15 Pandey, Y. N.; Papakonstantopoulos, G. J.; Doxastakis, M. Polymer/nanoparticle interactions: bridging the gap. *Macromolecules* **2013**, *46*, 5097–5106.
16 Volgin, I. V.; Larin, S. V.; Lyulin, S. V. Diffusion of nanoparticles in polymer systems. *Polym. Sci. Ser. C* **2018**, *60*, 122–134.
17 O'Reilly, M. V.; Winey, K. I. Silica nanoparticles densely grafted with PEO for ionomer plasticization. *RSC Adv.* **2015**, *5*, 19570–19580.
18 Shi, D. W.; Lai, X. L.; Jiang, Y. P.; Yan, C.; Liu, Z. Y.; Yang, W.; Yang, M. B. Synthesis of inorganic silica grafted three-arm PLLA and their behaviors for PLA matrix. *Chinese J. Polym. Sci.* **2019**, *37*, 216–226.
19 Purohit, P. J.; Huacuja-Sanchez, J. E.; Wang, D. Y.; Emmerling, F.; Thunemann, A.; Heinrich, G.; Schonhals, A. Structure-property relationships of nanocomposites based on polypropylene and layered double hydroxides. *Macromolecules* **2011**, *44*, 4342–4354.
20 Chen, L.; Zheng, K.; Tian, X. Y.; Hu, K.; Wang, R. X.; Liu, C.; Li, Y.; Cui, P. Double glass transitions and interfacial immobilized layer in *in-situ*-synthesized poly(vinyl alcohol)/silica nanocomposites. *Macromolecules* **2010**, *43*, 1076–1082.
21 Bogoslovov, R. B.; Roland, C. M.; Ellis, A. R.; Randall, A. M.; Robertson, C. G. Effect of silica nanoparticles on the local segmental dynamics in poly(vinyl acetate). *Macromolecules* **2008**, *41*, 1289–1296.
22 Schonhals, A.; Goering, H.; Costa, F. R.; Wagenknecht, U.; Heinrich, G. Dielectric properties of nanocomposites based on polyethylene and layered double hydroxide. *Macromolecules* **2009**, *42*, 4165–4174.
23 Lin, Y.; Liu, L. P.; Cheng, J. Q.; Shangguan, Y. G.; Yu, W. W.; Qiu, B. W.; Zheng, Q. Segmental dynamics and physical aging of polystyrene/silver nanocomposites. *RSC Adv.* **2014**, *4*, 20086–20093.
24 Rittigstein, P.; Torkelson, J. M. Polymer-nanoparticle interfacial interactions in polymer nanocomposites: confinement effects on glass transition temperature and suppression of physical aging. *J. Polym. Sci., Part B: Polym. Phys.* **2006**, *44*, 2935–2943.
25 Chakraborty, S.; Kumar, M.; Suresh, K.; Pugazhenthi, G. Investigation of structural, rheological and thermal properties of PMMA/Oni-AL LDH nanocomposites synthesized *via* solvent blending method: effect of LDH loading. *Chinese J. Polym. Sci.* **2016**, *34*, 739–754.
26 Rittigstein, P.; Priestley, R. D.; Broadbelt, L. J.; Torkelson, J. M. Model polymer nanocomposites provide an understanding of confinement effects in real nanocomposites. *Nat. Mater.* **2007**, *6*, 278.
27 Lin, Y.; Liu, L. P.; Xu, G. M.; Zhang, D. G.; Guan, A. G.; Wu, G. Z. Interfacial interactions and segmental dynamics of poly(vinyl acetate)/silica nanocomposites. *J. Phys. Chem. C* **2015**, *119*, 12956–12966.
28 Song, Y. H.; Bu, J.; Zuo, M.; Gao, Y.; Zhang, W. J.; Zheng, Q. Glass transition of poly(methyl methacrylate) filled with nanosilica and core-shell structured silica. *Polymer* **2017**, *127*, 141–149.
29 Kim, S. A.; Mangal, R.; Archer, L. A. Relaxation dynamics of nanoparticle-tethered polymer chains. *Macromolecules* **2015**, *48*, 6280–6293.
30 Park, C.; Ounaies, Z.; Watson, K. A.; Crooks, R. E.; Smith, J.; Lowther, S. E.; Connell, J. W.; Siochi, E. J.; Harrison, J. S.; Clair, T. L. S. Dispersion of single wall carbon nanotubes by in situ polymerization under sonication. *Chem. Phys. Lett.* **2002**, *364*, 303–308.
31 Zhu, B. K.; Xie, S. H.; Xu, Z. K.; Xu, Y. Y. Preparation and properties of the polyimide/multi-walled carbon nanotubes (MWNTs) nanocomposites. *Compos. Sci. Technol.* **2006**, *66*, 548–554.
32 Yen, C. T.; Chen, W. C.; Liaw, D. J.; Lu, H. Y. Synthesis and properties of new polyimide-silica hybrid films through both intrachain and interchain bonding. *Polymer* **2003**, *44*, 7079–7087.
33 Gong, G. M.; Gao, K.; Wu, J. T.; Sun, N.; Zhou, C.; Zhao, Y.; Jiang, L. A highly durable silica/polyimide superhydrophobic nanocomposite film with excellent thermal stability and abrasion resistant performances. *J. Mater. Chem. A* **2014**, *3*, 713–718.
34 Chang, C. C.; Chen, W. C. Synthesis and optical properties of polyimide-silica hybrid thin films. *Chem. Mater.* **2002**, *14*, 4242–4248.
35 Shen, J. J.; Zhang, D. G.; Liu, X.; Tang, Y. C.; Lin, Y.; Wu, G. Z. Facile fabrication of high-performance polyimide nanocomposites with *in situ* formed "impurity-free" dispersants. *Chinese J. Polym. Sci.* **2016**, *34*, 532–541.
36 Jian, S. J.; Hu, X. W.; Zou, Y.; Chen, S. L.; Hou, H. Q. The preparation and characterization for high-strength electrospun polyimide/Ag composite nanofibers. *J. Jiangxi. Normal. Univ: Nat. Sci. Ed.* **2012**, *36*, 1–4.
37 Yu, Q. Q.; Qi, S. L.; Wu, D. Z.; Wang, X. D.; Jin, R. G.; Wu, Z. P.

Febrication of surface-nickelized polyimide composite films by surface modification and *in situ* reduction method. *Polym. Mater. Sci. Eng.* **2012**, *28*, 152–154.
38 Hsu, C. T.; Wu, C.; Chuang, C. N.; Chen, S. H.; Chiu, W. Y.; Hsieh, K. H. Synthesis and characterization of nano silver-modified graphene/PEDOT:PSS for highly conductive and transparent nanocomposite films. *J. Polym. Res.* **2015**, *22*, 200.
39 Wu, G. Z.; Li, B. P.; Jiang, J. D. Carbon black self-networking induced co-continuity of immiscible polymer blends. *Polymer* **2010**, *51*, 2077–2083.
40 Torquato, S.; Hyun, S.; Donev, A. Multifunctional composites: Optimizing microstructures for simultaneous transport of heat and electricity. *Phys. Rev. Lett.* **2002**, *89*, 266601.
41 Ragosta, G.; Abbate, M.; Musto, P.; Scarinzi, G. Effect of the chemical structure of aromatic polyimides on their thermal aging, relaxation behavior and mechanical properties. *J. Mater. Sci.* **2012**, *47*, 2637–2647.
42 Meador, M. A. B.; McMillon, E.; Sandberg, A.; Barrios, E.; Wilmoth, N. G.; Mueller, C. H.; Miranda, F. A. Dielectric and other properties of polyimide aerogels containing fluorinated blocks. *ACS Appl. Mater. Intefaces* **2014**, *6*, 6062–6068.
43 Marques, M. E.; Mansur, A. A. P.; Mansur, H. S. Chemical functionalization of surfaces for building three-dimensional engineered biosensors. *Appl. Surf. Sci.* **2013**, *275*, 347–360.
44 Park, S. J.; Cho, K. S.; Kim, S. H. A study on dielectric characteristics of fluorinated polyimide thin film. *J. Colloid. Interf. Sci.* **2004**, *272*, 384–390.
45 Wolany, D.; Fladung, T.; Duda, L.; Lee, J. W.; Gantenfort, T.; Wiedmann, L.; Benninghoven, A. Combined ToF-SIMS/XPS study of plasma modification and metallization of polyimide. *Surf. Interface Anal.* **1999**, *27*, 609–617.
46 Iyer, K. S.; Luzinov, I. Effect of macromolecular anchoring layer thickness and molecular weight on polymer grafting. *Macromolecules* **2005**, *37*, 9538–9545.
47 Liu, H.; Zhao, H.Y.; Florian, M. P.; Qian, H. J.; Sun, Z. Y.; Lu, Z. Y. Distribution of the number of polymer chains grafted on nanoparticles fabricated by grafting-to and grafting-from procedures. *Macromolecules* **2018**, *51*, 3758–3766.
48 Xing, J. Y.; Lu, Z. Y.; Liu, H.; Xue, Y. H. The selectivity of nanoparticles for polydispersed ligand chains during the grafting-to process: a computer simulation study. *Phys. Chem. Chem. Phys.* **2018**, *20*, 2066–2074.
49 Wang, W.; Wu, J. S. Interfacial influence on mechanical properties of polypropylene/polypropylene-grafted silica nanocomposites. *J. Appl. Polym. Sci.* **2018**, *135*, 45887.
50 Iyer, K. S.; Zdyrko, B.; Malz, H.; Pionteck, J.; Luzinov, I. Polystyrene layers grafted to macromolecular anchoring layer. *Macromolecules* **2003**, *36*, 6519–6526.
51 Llorente, A.; Serrano, B.; Baselga, J. The effect of polymer grafting in the dispersibility of alumina/polysulfone nanocomposites. *Macromol. Res.* **2016**, *25*, 1–10.
52 Lin, Y.; Hu, S. N.; Wu, G. Z. Structure, dynamics and mechanical properties of polyimide-grafted silica nanocomposites. *J. Phys. Chem. C* **2019**, *123*, 6616–6626.
53 Grala, M.; Bartczak, Z.; Różański, A. Morphology, thermal and mechanical properties of polypropylene/$SiO_2$ nanocomposites obtained by reactive blending. *J. Polym. Res.* **2016**, *23*, 25.
54 Natarajan, B.; Neely, T.; Rungta, A.; Benicewicz, B. C.; Schadler, L. S. Thermomechanical properties of bimodal brush modified nanoparticle composites. *Macromolecules* **2013**, *46*, 4909–4918.
55 Ferreira, P. G.; Ajdari, A.; Leibler, L. Scaling law for entropic effects at interfaces between grafted layers and polymer melts. *Macromolecules* **1998**, *31*, 3994–4003.
56 Chao, H.; Riggleman, R. A. Effect of particle size and grafting density on the mechanical properties of polymer nanocomposites. *Polymer* **2013**, *54*, 5222–5229.

https://doi.org/10.1007/s10118-019-2300-6